

## Mn<sup>2+</sup> Intercalated V<sub>2</sub>C MXene for Enhanced Sodium Ion Battery

WEI Shi-Qiang, WANG Chang-Da, ZHANG Peng-Jun, ZHU Ke-Fu, CHEN Shuang-Ming, SONG Li

(National Synchrotron Radiation Laboratory, CAS Center for Excellence in Nanoscience, University of Science and Technology of China, Hefei 230029, China)

**Abstract:** Mn<sup>2+</sup> intercalation strategy to optimize the sodium storage performance of V<sub>2</sub>C MXene was studied. The intercalated Mn<sup>2+</sup> not only enlarged the interlayer spacing of V<sub>2</sub>C MXene but also formed a V–O–Mn covalent bond, which was beneficial to stabilize the structure of V<sub>2</sub>C and inhibit the structural collapse caused by volume change during Na<sup>+</sup> deintercalation or intercalation. As a result, the intercalated V<sub>2</sub>C MXene (V<sub>2</sub>C@Mn) electrode showed a high specific capacity of 425 mAh·g<sup>-1</sup> at the current density of 0.05 A·g<sup>-1</sup>, and 70% retention after 1200 cycles. This result clearly suggests that cations intercalated MXene has a great prospect in Na<sup>+</sup> storage.

**Key words:** layered material; V<sub>2</sub>C MXene; Na<sup>+</sup> storage; metal cation intercalation; XAFS

There is a growing desire to develop renewable and clean energy, due to environmental problems such as pollution caused by fossil fuels<sup>[1]</sup>. Sodium ion battery (SIB) is spurring rapid development as a substitute for lithium ion battery because of the abundance of Na resources, low cost and similar working mechanism<sup>[2-3]</sup>. However, the design of sodium ion devices with excellent properties is not easy as the lack of appropriate anode materials restricted by the larger radius of sodium ion than lithium ion (0.102 nm vs 0.076 nm)<sup>[4]</sup>. This will result in sluggish kinetics of sodium ions and structural collapse of the electrode material during charge and discharge cycles. For instance, graphite, a commercialized lithium ion battery anode material, is not suitable for the negative electrode of SIB<sup>[5]</sup>.

In recent years, some advancements have been made on the anode materials of Na ion battery. Like metal tin has been proved as high specific capacity anode material, but impeded its practical application due to huge volume change during its working process<sup>[6]</sup>. Transition metal carbides and nitrides (MXenes) are promising for energy storage since its discovery in 2011 in terms of its metallic electrical conductivity, large electrochemically active surface and unique layered structure<sup>[7-9]</sup>. Currently, the most widely studied MXenes for Na<sup>+</sup> storage are Ti<sub>3</sub>C<sub>2</sub><sup>[10-11]</sup>. However, it has been proved that V<sub>2</sub>C MXene is also one of the most promising electrode materials due

to its smaller atomic mass<sup>[12]</sup>. Even though, only a few V<sub>2</sub>C MXene works for NIB are reported due to the difficulties in sample preparation and low capacity. For example, Yang, *et al.*<sup>[13]</sup> reported the storage mechanism of sodium ion intercalation between interlayers of vanadium carbide with a small capacity about 125 mAh·g<sup>-1</sup> at 10 mA·g<sup>-1</sup>, which is still a gap between practical applications. Our previous works have proven that the Li<sup>+</sup> storage performance of V<sub>2</sub>C MXene can be improved by intercalation of cobalt and tin ions<sup>[14-15]</sup>. It paved a path to improve the performance of V<sub>2</sub>C based sodium ion battery in both specific capacity and cycle stability through metal cations intercalation.

In the present study, we reported the intercalation of transition metal ions of manganese into layered V<sub>2</sub>C MXene by ion exchange method, labeled as V<sub>2</sub>C@Mn. Mn<sup>2+</sup> was successfully decorated into the interlayer of V<sub>2</sub>C MXene and formed V–O–Mn bond according to the analysis of XRD, XAS, TEM and Element Mapping characterizations. It was demonstrated that the V<sub>2</sub>C@Mn electrodes exhibited high specific capacity and outstanding cycling performance for SIB.

## 1 Experimental

### 1.1 Synthesis of V<sub>2</sub>C and V<sub>2</sub>C@Mn MXenes

As discussed in our previous articles, V<sub>2</sub>C MXene was

**Received date:** 2019-06-03; **Revised date:** 2019-07-15

**Foundation item:** National Key R&D Program of China (2017YFA0303500); National Natural Science Foundation of China (11574280, 21727801, 11605201, U1632151); National Postdoctoral Program for Innovative Talents (BX 20190315); NSFC-MAECI (51861135202); CAS Key Research Program of Frontier Sciences (QYZDB-SSW-SLH018); Fundamental Research Funds for the Central Universities (WK2310000074)

**Biography:** WEI Shi-Qiang(1994–), male, Master candidate. E-mail: sqw@mail.ustc.edu.cn

魏世强(1994–), 男, 硕士研究生. E-mail: sqw@mail.ustc.edu.cn

**Corresponding author:** CHEN Shuang-Ming, associate professor. E-mail: csm@ustc.edu.cn

陈双明, 副研究员. E-mail: csm@ustc.edu.cn

synthesized through selectively etching  $V_2AlC$  MAX powders, which were synthesized by calcining the ball-milled V, Al and C powders under  $1500\text{ }^\circ\text{C}$  in argon atmosphere. To obtain  $K^+$  intercalated  $V_2C$  ( $V_2C@K$ ) MXene, about 500 mg as-prepared  $V_2C$  powders were immersed in 20 mL 0.2 mol/L KOH aqueous solution followed by stirring for 2 d at  $45\text{ }^\circ\text{C}$ . Afterwards, the solution was centrifuged by using deionized water and ethanol for several times. Then  $V_2C@K$  was obtained after freeze-drying overnight.  $V_2C@Mn$  was prepared by soaking  $V_2C@K$  in 0.2 mol/L  $Mn(NO_3)_2$  through ion exchange between manganese ions and  $K^+$ .

## 1.2 Material characterization

The morphology of  $V_2C@Mn$  was presented with a field emission SEM (SU8220) and a TEM (JEOL JEM2010), elemental mapping images were also carried out with SEM (SU8220). X-ray diffraction (XRD) patterns were measured by a Sample horizontal high power X-ray diffractometer (Rigaku TTRIII) with  $Cu\ K\alpha$  radiation ( $\lambda=0.154\text{ nm}$ ). Chemical compositions of  $V_2C@Mn$  were analyzed by high-resolution XPS recorded with a Synchrotron Radiation Photoelectron Spectrometer Station Equipment in Hefei by using  $Mg\ K\alpha$  X-ray ( $h\nu=1253\text{ eV}$ ). V L-edge and O K-edge XANES measurements were performed at the beamline BL12B-a (CMD) in Hefei Synchrotron Radiation Equipment. The Mn K-edge XAFS measurement was performed in the fluorescence mode at the beamline 1W1B in Beijing Synchrotron Radiation Facility (BSRF).

## 1.3 Electrochemical measurements

The working electrodes of  $V_2C@Mn$  and  $V_2C$  MXenes were prepared by mixing  $V_2C@Mn$  or  $V_2C$  MXene (70%), acetylene black (ACET 20%), and polyvinylidene fluoride (PVDF, 10%). Then it was coated on a copper foil after uniformly grinding in *N*-methyl-2-pyrrolidone (NMP) and dried in vacuum oven overnight. The batteries were assembled in an Ar filled glove box (MBraun, Germany) into coin cells (CR2032) with sodium tablets as the counter electrodes, glass fiber as the separators and 1 mol/L  $NaClO_4$  in (EC: DMC, vs. 1 : 1) as the electrolyte. Rate capability and cycle ability were achieved on a Land CT2001A cell test system at  $25\text{ }^\circ\text{C}$  in the potential range between 0.01 and 3 V. Meanwhile, cyclic voltammetry (CV) at scan rate from 0.1 to  $1.0\text{ mV}\cdot\text{s}^{-1}$  in the same voltage range was performed on the CHI660D electrochemical workstation.

# 2 Results and discussion

## 2.1 Structure characterization

$V_2C$  powders were produced by selectively etching out

the Al atomic layer from the MAX phase. During etching, the surface would be functionalized with hydroxyl, oxygen or fluorine terminations, so it has a formulation  $V_2CT_x$  ( $T_x=F, O, OH$ ). Transition metal ions of manganese entered the vanadium carbide layers by replacing the potassium ions which were intercalated into  $V_2C$  MXene because of the etching effect of KOH. Manganese ions could shore up the layers of  $V_2C$  MXenes during the charge and discharge process which could prevent the structural collapse and accelerate ion diffusion.

As illustrated in Fig. 1(a), the X-ray diffraction (XRD) image shows a typical (0002) peak of  $V_2C$  MXene around  $12^\circ$  with some  $V_2AlC$  residue after HF treatment. After stirring in KOH solution, the (0002) peak shifts toward lower degree, which implies the expansion of the  $V_2C@K$  MXene interplaner. According to Bragg equation, the interlayer spacing of  $V_2C@K$  MXene is about 0.96 nm. Interestingly, after the replacement of  $K^+$  by  $Mn^{2+}$ , the interlayer spacing of  $V_2C@Mn$  decreases to approximately 0.95 nm compared with  $V_2C@K$ . This weak contraction can be attributed to greater electrostatic attraction of bivalent Mn ion than monovalent K ion. Similar shrinkage is also observed in Co, Sn intercalated MXenes<sup>[14-15]</sup>. SEM image of  $V_2C@Mn$  in Fig. 1(b) shows that the  $V_2C@Mn$  preserved layer structure which is similar to the original structure of  $V_2C$ , indicating that there is no obvious structure collapse after Mn ion intercalation. Elements mapping shows the uniform distribution of V, O and Mn. The layered structure of  $V_2C@Mn$  is also presented in the HRTEM image (Fig. 1(c)), it shows a interlayer spacing of 0.95 nm which is consistent with XRD results. The ICP-AES indicates that the element composition of V, Al and K for  $V_2C$ -KOH from ICP is 100.5, 1.765 and  $8.683\text{ }\mu\text{g}\cdot\text{mL}^{-1}$ , corresponding to 70.70wt%, 1.20wt% and 6.11wt%, respectively. For  $V_2C@Mn$ , the ICP results for V, Al, K and Mn atoms were 106.5, 1.529, 2.489 and  $7.61\text{ }\mu\text{g}\cdot\text{mL}^{-1}$ , corresponding to 71.89wt%, 1.0wt%, 1.16wt% and 5.00wt%, respectively. It can be concluded that nearly all of K was successfully substituted by Mn, and few adsorptive or intercalated K ions remained. In short, manganese ions successfully intercalated into  $V_2C$  MXene and enlarged the interlayer spacing which may stable the structure and accelerate ion transmission.

The intercalation of manganese ions was investigated by X-ray photoelectron spectroscopy (XPS) and X-ray absorption fine spectroscopy (XAFS) as shown in Fig. 2. In the high resolution Mn2p spectrum, two predominant Mn2p<sub>3/2</sub> peaks are located at 641.3 and 643.2 eV, corresponding to divalent manganese ions and trivalent manganese ions<sup>[16]</sup>. Among them, divalent manganese ions account for the majority, and trivalent manganese ions

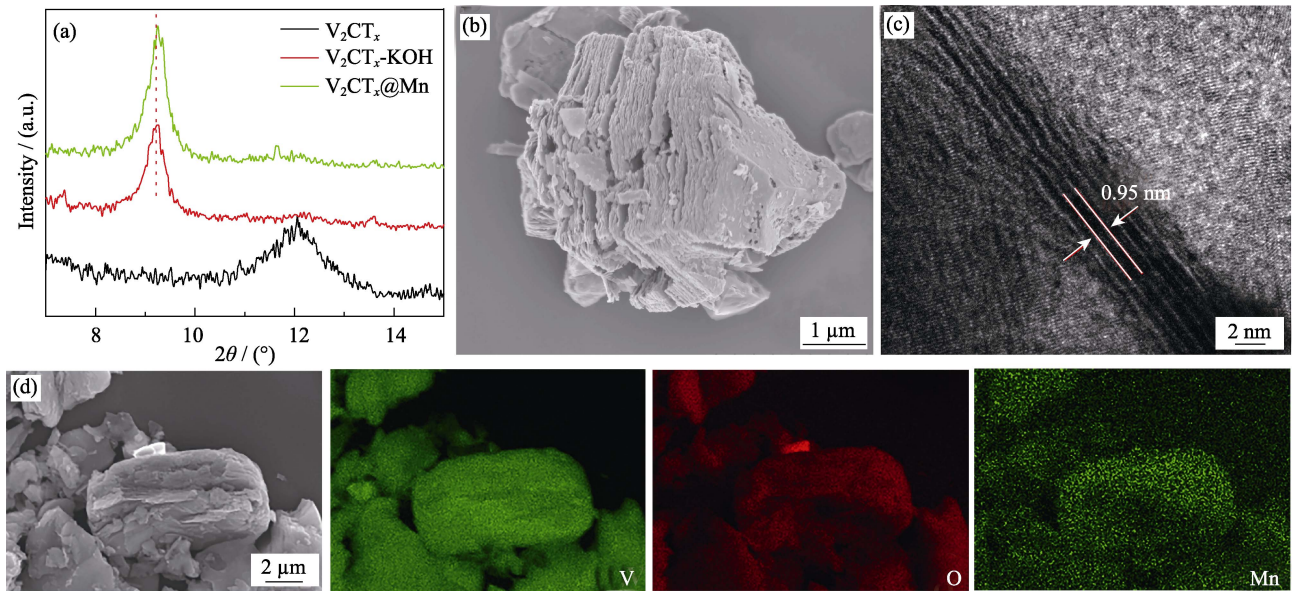


Fig. 1 Morphological characterization of V<sub>2</sub>C@Mn

(a) XRD patterns of V<sub>2</sub>C, V<sub>2</sub>C-K and V<sub>2</sub>C@Mn; (b) SEM image of as-prepared V<sub>2</sub>C@Mn; (c) TEM image of as prepared V<sub>2</sub>C@Mn; (d) Elements mapping of V<sub>2</sub>C@Mn, from left to right: scanning area map of V, O and Mn

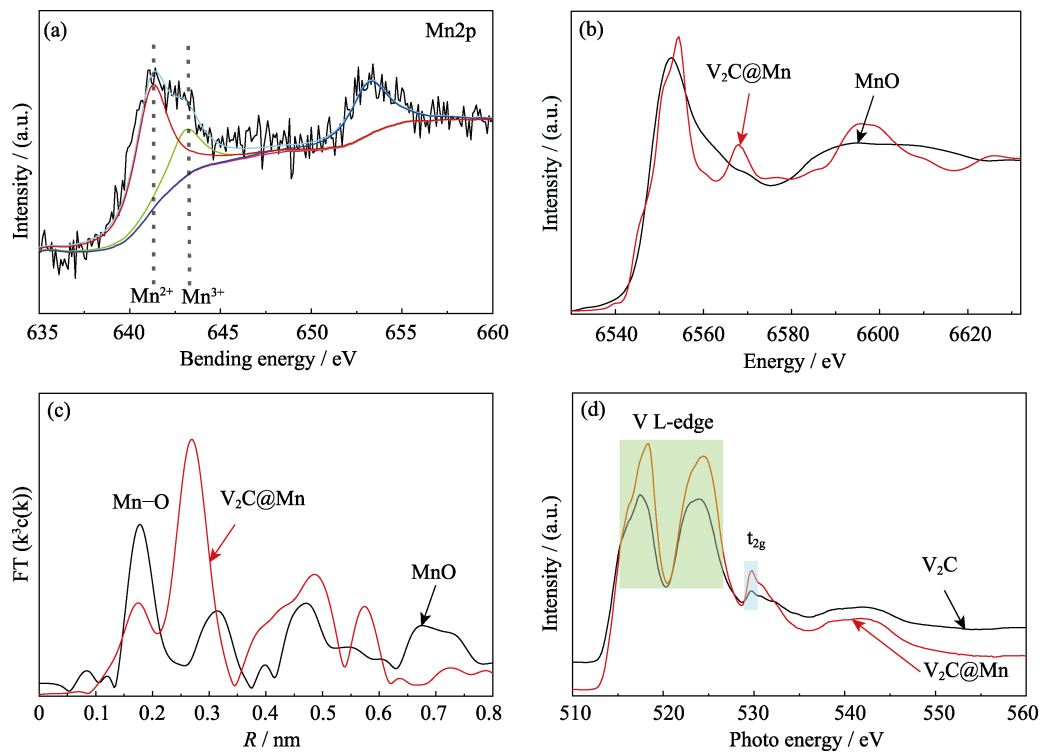


Fig. 2 Structural characterization of V<sub>2</sub>C@Mn MXene

(a) High resolution XPS of manganese; (b) Spectra of XANES for V<sub>2</sub>C@Mn MXene and MnO standard sample; (c) Fourier-transformed Mn K-edge EXAFS spectra of V<sub>2</sub>C@Mn MXene and MnO standard sample; (d) V L-edge and O K-edge XANES spectra of pure V<sub>2</sub>C MXene and V<sub>2</sub>C@Mn MXene

have only a small part. It can be clearly verified by the Mn K-edge XANES results of V<sub>2</sub>C@Mn MXene and MnO as shown in Fig. 2(b). The absorption edge position of Mn K-edge XANES spectrum of V<sub>2</sub>C@Mn is very close to that of the MnO, which indicates that almost all of the manganese ions are divalent rather than trivalent.

XPS and XAFS are powerful experimental technology for explanation the valence and spin states of transition-metal ion in the solids<sup>[17]</sup>. The former mainly gives the valence information within 10 nm of the material surface, while the latter gives the average information of the whole material. Thus, it can be concluded that most of

the  $\text{Mn}^{2+}$  are intercalated inside the interlayer, while some  $\text{Mn}^{3+}$  located on the near surface of  $\text{V}_2\text{C}$  MXene because of the easier oxidation. The corresponding Fourier-transformed EXAFS spectra in Fig. 2(c) clearly displays the Mn-O peak of  $\text{V}_2\text{C}@\text{Mn}$  compared with MnO, indicating the formation of Mn-O bond.

To study more detailed electronic structure information of  $\text{V}_2\text{C}@\text{Mn}$ , V L-edge and O K-edge XANES spectra were performed (Fig. 2(d)). For the V L-edge, there are two peaks located at 518 and 525 eV, corresponding to the spin-orbit (SO) split  $L_3(2p_{3/2})$  and  $L_2(2p_{1/2})$  parts, respectively. It is obvious that the shape of two curves are very similar except that the peak position shifted to higher energy after  $\text{Mn}^{2+}$  intercalation. As we know, this shift refers to the elevated valence of V ions. Due to crystal field splitting, the O K-edge can be divided into two parts. The first part is the region of  $\text{O}2p\text{-V}3d(t_{2g})$  and  $\text{O}2p\text{-V}3d(e_g)$  at lower energy. The second part is the region at higher energy about 542 eV, associated with the mixture of  $\text{O}2p$  with  $\text{V}4s$ <sup>[18-19]</sup>. The  $\text{O}2p$  orbitals are greatly mixed with  $\text{V}3d$  orbitals, resulting in a wide distribution and strong absorption signal which clearly demonstrates the significant covalent nature of the V-O bonds in the  $\text{V}_2\text{C}$  and  $\text{V}_2\text{C}@\text{Mn}$  MXene. After  $\text{Mn}^{2+}$  intercalation, the energy of second part shifted to lower position because of the transitions toward hybridized levels

between  $\text{Mn}4s$  and V-O hybridization<sup>[20]</sup>, corresponding to the observed shift of V edge to a higher energy. This indicates the formation of Mn-O bonds. Therefore, combining with all of the above analysis results we can convince the conformation of V-O-Mn bond in  $\text{V}_2\text{C}@\text{Mn}$  MXene.

## 2.2 Na ion storage performance

In order to evaluate the electrochemical properties of the  $\text{Mn}^{2+}$  intercalated  $\text{V}_2\text{C}$  as anode material for NIB, 2032 coin-type cells with Na foil as counterparts were assembled. Fig. 3(a) shows the cyclic voltammetry (CV) graph of  $\text{V}_2\text{C}@\text{Mn}$  MXene electrode at scan rate from 0.1 to  $1.0 \text{ mV}\cdot\text{s}^{-1}$ . At low scan rate  $0.1 \text{ mV}\cdot\text{s}^{-1}$ , there are a pair of wide redox peaks at approximately 1.5/1.8 V after the initial cycle. As the sweep rates increased, the redox peaks become more pronounced. More intuitively, all the CV curves display a quasi-rectangle shape, which indicates a typical pseudocapacitive behavior of  $\text{V}_2\text{C}$  MXene for NIB. In order to add more persuasive insight, we calculated the  $b$  from anodic and cathodic currents. The  $b$  from anodic and cathodic currents are about 0.75 and 0.79 respectively, clearly indicating the storage mechanism is mainly pseudocapacitive behavior. Our CV result is similar to other works where  $\text{V}_2\text{C}$  MXene also shows pseudo-capacitive behavior in  $\text{Na}^+$  storage<sup>[21]</sup>. The high and irreversible cathodic current below 1 V might

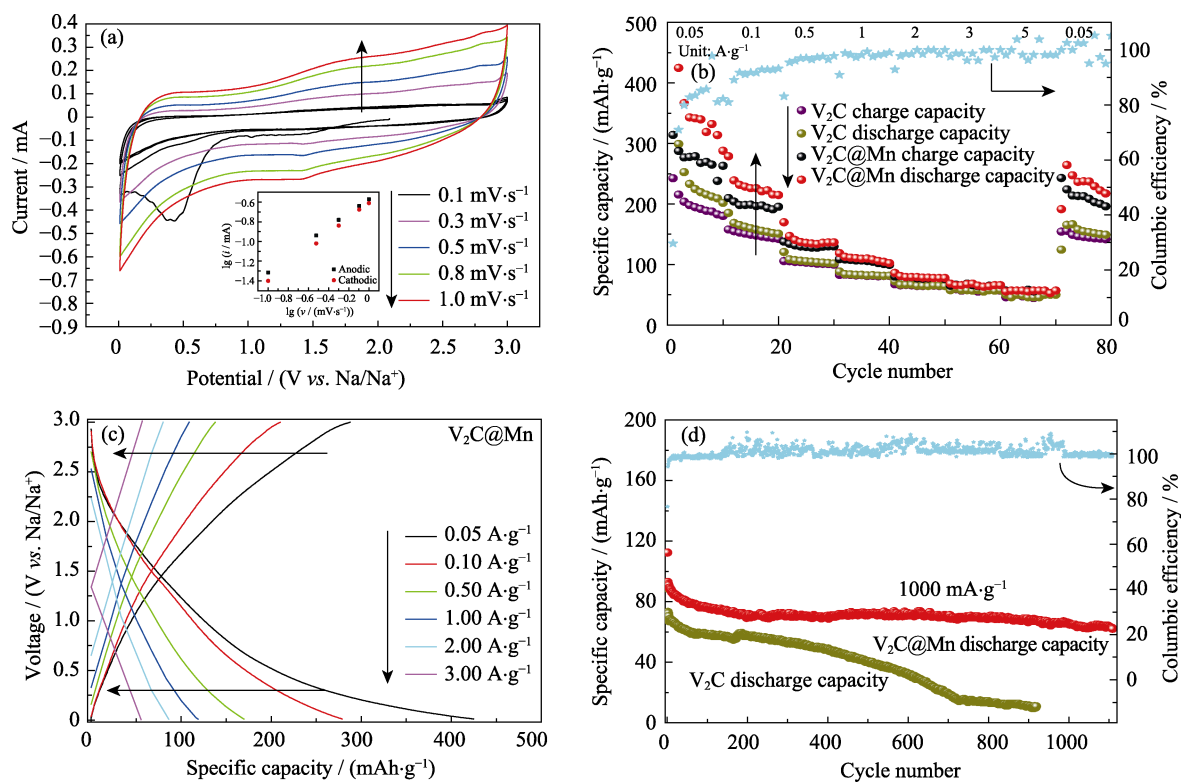


Fig. 3 Electrochemical performance in half-cell

(a) CV curves of  $\text{V}_2\text{C}@\text{Mn}$  MXene electrode at the scan rate from 0.1 to  $1.0 \text{ mV}\cdot\text{s}^{-1}$ ; (b) Rate performance of  $\text{V}_2\text{C}@\text{Mn}$  and pure  $\text{V}_2\text{C}$  electrodes at different current densities; (c) Charge and discharge profiles of  $\text{V}_2\text{C}@\text{Mn}$  at different current densities; (d) Cycle stabilities of  $\text{V}_2\text{C}@\text{Mn}$  and pure  $\text{V}_2\text{C}$  electrodes at the current density of  $1000 \text{ mA}\cdot\text{g}^{-1}$ . Inset in (a) is the variation of  $\lg i$  versus  $\lg v$

be ascribed to the formation of solid electrolyte interphase (SEI) and the decomposition of electrolyte in the first cycle<sup>[22]</sup>.

To meet the demand of fast charge and release of energy storage devices, the rate and cycle performance of devices are extremely important. As shown in Fig 3(b), the V<sub>2</sub>C@Mn electrode not only delivers higher specific capacity than pure V<sub>2</sub>C electrode, but also shows better rate performance. Even under high current density of 5 A·g<sup>-1</sup>, V<sub>2</sub>C@Mn electrode can still deliver a capacity of 60 mAh·g<sup>-1</sup>, but for V<sub>2</sub>C electrode, it is only about 50 mAh·g<sup>-1</sup>. Fig. 3(c) shows the charge and discharge curves of V<sub>2</sub>C@Mn MXene at current densities from 0.05 to 5 A·g<sup>-1</sup>. There are about 425, 280, 170, 120, 86 and 56 mAh·g<sup>-1</sup> under 0.05, 0.1, 0.5, 1, 2, 5 A·g<sup>-1</sup>, respectively. The shapes of charge and discharge curves are approximate slash and there are no platforms with the increase of current densities, which were consistent with CV results. The behavior demonstrates that the Na<sup>+</sup> storing mechanism of V<sub>2</sub>C@Mn MXene is mainly capacitive behavior and with the current density increases, the contribution of capacitance also increases. More intuitively, the superiority of V<sub>2</sub>C@Mn MXene to V<sub>2</sub>C MXene is reflected in the cycle stability. After rate performance test, both of the two electrodes are carried on cycling test as shown in Fig. 3(d). There is still 70% of discharge capacity remained after 1200 long-term cycles for V<sub>2</sub>C@Mn electrode. In contrast, the specific capacity of pure V<sub>2</sub>C electrode decays very fast, only 20% capacity is preserved after 800 cycles. The higher specific capacity, more excellent rate performance and superior cycle stability of V<sub>2</sub>C@Mn are benefited from the intercalation of Mn<sup>2+</sup> into V<sub>2</sub>C MXene layers which stabilizes the structure and accelerates ion transmission.

The dynamics of intercalated Mn<sup>2+</sup> was investigated by *ex-situ* X-ray photoelectron spectroscopy (XPS) at different charge and discharge voltages. As shown in Fig. 4, the intensity of the peaks corresponding to Mn<sup>2+</sup> are weakened as the charging voltage increased while the peaks corresponding to Mn<sup>3+</sup> increase, indicating that Mn<sup>2+</sup> is oxidized to Mn<sup>3+</sup> during charging process. On the contrary, the Mn<sup>3+</sup> is reduced to Mn<sup>2+</sup> during discharging process. It can be concluded that Mn ions intercalation strategy not only stabilizes the structure of V<sub>2</sub>C MXene, but also increases the pseudo-capacity.

### 3 Summary

In summary, Mn<sup>2+</sup> intercalated V<sub>2</sub>C MXene was successfully synthesized through ion exchange method. By using XRD, element mapping, XPS, and XAFS characterization techniques, it can be proved that the intercalated

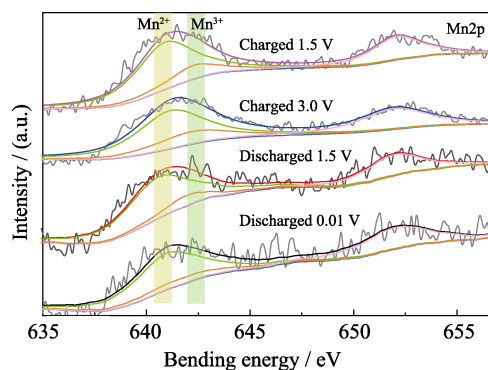


Fig. 4 *Ex-situ* X-ray photoelectron spectroscopy at different charge and discharge voltages

Mn<sup>2+</sup> not only enlarged the interlayer spacing of V<sub>2</sub>C MXene but also formed a V–O–Mn covalent bond in the interlayer, which were beneficial to improve the Na<sup>+</sup> storage capacity and stabilize the structure of V<sub>2</sub>C MXene volume change. The results showed that V<sub>2</sub>C@Mn electrode can deliver a high specific capacity of 425 mAh·g<sup>-1</sup> at current density of 0.05 A·g<sup>-1</sup>. Notably, over 70% capacity was still remaining after 1200 long-term cycles. We believe that ion intercalation can promote the highly development of MXene based Na<sup>+</sup> storage.

### References

- [1] LUO J M, FANG C, JIN C B, *et al.* Tunable pseudocapacitance storage of MXene by cation pillaring for high performance sodium-ion capacitors. *Journal of Materials Chemistry A*, 2018, **6**(17): 7794–7806.
- [2] LUO J M, ZHENG J H, NAI J W, *et al.* Atomic sulfur covalently engineered interlayers of Ti<sub>3</sub>C<sub>2</sub> MXene for ultra-fast sodium-ion storage by enhanced pseudocapacitance. *Advanced Functional Materials*, 2019, **29**(10): 1808107.
- [3] KAJIYAMA S, SZABOVA L, SODEYAMA K, *et al.* Sodium-ion intercalation mechanism in MXene nanosheets. *ACS Nano*, 2016, **10**(3): 3334–3341.
- [4] DONG Y, WU Z S, ZHENG S H, *et al.* Ti<sub>3</sub>C<sub>2</sub> MXene-derived sodium/potassium titanate nanoribbons for high-performance sodium/potassium ion batteries with enhanced capacities. *ACS Nano*, 2017, **11**(5): 4792–4800.
- [5] LUO W, SHEN F, BOMMIER C, *et al.* Na-ion battery anodes: materials electrochemistry. *Accounts of Chemical Research*, 2016, **49**(2): 231–240.
- [6] ZHANG Y, ZHU P, HUANG L, *et al.* Few-layered SnS<sub>2</sub> on few-layered reduced graphene oxide as Na-ion battery anode with ultralong cycle life and superior rate capability. *Advanced Functional Materials*, 2015, **25**(3): 481–489.
- [7] ANASORI B, LUKATSKAYA M R, GOGOTSI Y. 2D metal carbides and nitrides (MXenes) for energy storage. *Nature*, 2017, **2**: 16098.
- [8] PENG J H, CHEN X Z, ONJ W J, *et al.* Surface and heterointerface engineering of 2D MXenes and their nanocomposites: insights into electro- and photocatalysis. *Chem*, 2018, **5**: 1–33.
- [9] KHAZAEI M, RANJBAR A, ARAI M, *et al.* Electronic properties and applications of MXenes: a theoretical review. *Journal of Materials Chemistry A*, 2017, **5**: 2488–2503.
- [10] ER D, LI J, NAGUIB M, *et al.* Ti<sub>3</sub>C<sub>2</sub> MXene as a high capacity

- electrode material for metal (Li, Na, K, Ca) ion batteries. *ACS Applied Material Interfaces*, 2014, **6**(14): 11173–11179.
- [11] LI J, YAN D, HOU S, *et al.* Improved sodium-ion storage performance of  $Ti_3C_2T_x$  MXenes by sulfur doping. *Journal of Materials Chemistry A*, 2018, **6**(3): 1234–1243.
- [12] ZHU J J, SCHWINGENSCHLÖGL U. P and Si functionalized MXenes for metal-ion battery applications. *2D Materials*, 2017, **4**: 025073.
- [13] BAK S M, QIAO R M, YANG W L, *et al.* Na-ion intercalation and charge storage mechanism in 2D vanadium carbide. *Advance Energy Materials*, 2017, **7**(20): 1700959.
- [14] WANG C D, XIE H, CHEN S M, *et al.* Atomic cobalt covalently engineered interlayers for superior lithium-ion storage. *Advanced Materials*, 2018, **30**(32): 1802525.
- [15] WANG C D, CHEN S M, XIE H, *et al.* Atomic  $Sn^{4+}$  decorated into vanadium carbide MXene interlayers for superior lithium storage. *Advance Energy Materials*, 2019, **9**(4): 1802977.
- [16] DU Y, HUA Z, HUANG W, *et al.* Mesostructured amorphous manganese oxides: facile synthesis and highly durable elimination of low-concentration NO at room temperature in air. *Chemical Communications*, 2015, **51**(27): 5887–5889.
- [17] KANG J S, HWANG J, KIM D H, *et al.* Soft X-ray magnetic circular dichroism study of valence and spin states in  $FeT_2O_4$  (T=V, Cr) spinel oxides. *Journal of Applied Physics*, 2013, **113**(17): 17E116.
- [18] YE Y F, KAPILASHRAMI M, CHUANG C H, *et al.* X-ray spectroscopies studies of the 3d transition metal oxides and applications of photocatalysis. *MRS Communications*, 2017, **7**(1): 53–66.
- [19] JANG W L, LU Y M, CHEN C L, *et al.* Local geometric and electronic structures of gasochromic  $VO_x$  films. *Physical Chemistry Chemical Physics*, 2014, **16**(10): 4699–4708.
- [20] FILATOVA E O, BARABAN A P, KONASHUK A S, *et al.* Transparent-conductive-oxide (TCO) buffer layer effect on the resistive switching process in metal/ $TiO_2$ /TCO/metal assemblies. *New Journal of Physics*, 2014, **16**(11): 113014.
- [21] DALL'AGNESE Y, TABERNA P L, GOGOTSI Y, *et al.* Two-dimensional vanadium carbide (MXene) as positive electrode for sodium-ion capacitors. *The Journal of Physical Chemistry Letters*, 2015, **6**(12): 2305–2309.
- [22] GE Y, PAN P F, PENG X, *et al.* Dual-confined sulfur cathodes encapsulated in  $MnO_2$  nanotubes and wrapped with PEDOT for high-performance lithium-sulfur batteries. *Chinese Journal of Inorganic Chemistry*, 2019, **39**(5): 769–779.

## $Mn^{2+}$ 插层 $V_2C$ MXene 应用于钠离子电池的研究

魏世强, 王昌达, 张鹏军, 朱可夫, 陈双明, 宋礼

(中国科学技术大学 中国科学院纳米科学卓越中心, 国家同步辐射实验室, 合肥 230029)

**摘要:** 本研究提出一种  $Mn^{2+}$  插层策略用于优化  $V_2C$  MXene 的储钠性能。 $Mn^{2+}$  的插层不仅扩大了  $V_2C$  MXene 的层间距同时形成了 V–O–Mn 共价键, 有利于稳定  $V_2C$  的结构, 抑制  $Na^+$  脱嵌过程中由于体积变化引起的结构坍塌。结果表明, 插层后的  $V_2C$  MXene( $V_2C@Mn$ ) 电极在电流密度为  $0.05 A \cdot g^{-1}$  时具有  $425 mAh \cdot g^{-1}$  的高比容量, 并且经过 1200 次长循环后容量还有 70% 保留。 $V_2C@Mn$  优异的性能表明阳离子插层调控的 MXene 在  $Na^+$  存储方面具有潜在的应用前景。

**关键词:** 层状材料;  $V_2C$  MXene; 钠离子存储; 金属阳离子插层; 同步辐射吸收谱

中图分类号: TQ174 文献标识码: A